NANO LETTERS
Letter
Cite This: Nano Lett. 2019, 19, 1318−1325
pubs.acs.org/NanoLett

Copper's Role in the Photoluminescence of $Ag_{1-x}Cu_xInS_2$ Nanocrystals, from Copper-Doped $AgInS_2$ ($x \sim 0$) to $CuInS_2$ ($x = 1$)

Kira E. Hughes, Sarah R. Ostheller, Heidi D. Nelson, and Daniel R. Gamelin*

Department of Chemistry, University of Washington, Seattle, Washington 98195-1700, United States

Supporting Information

ABSTRACT: A series of $Ag_{1-x}Cu_xInS_2$ nanocrystals (NCs) spanning from $0 \leq x \leq \sim 1$ was synthesized by partial cation exchange to identify copper's contributions to the electronic structure and spectroscopic properties of these NCs. Discrete midgap states appear above the valence band upon doping $AgInS_2$ NCs with Cu^+ (small x). Density functional theory calculations confirm that these midgap states are associated with the 3d valence orbitals of the Cu^+ impurities. With increasing x, these impurity d levels gradually evolve to become the valence-band edge of $CuInS_2$ NCs, but the highest-occupied orbital's description does not change significantly across the entire range of x.

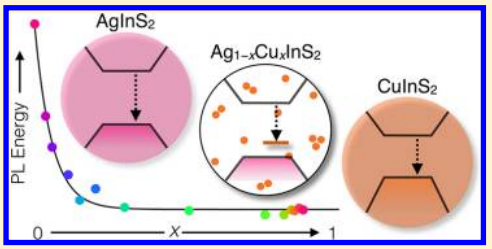

In contrast with this gradual evolution, $Ag_{1-x}Cu_xInS_2$ NC photoluminescence shifts rapidly with initial additions of Cu^+ (small x) but then becomes independent of x beyond $x > \sim 0.20$, all the way to $CuInS_2$ ($x = 1.00$). Data analysis suggests small but detectable hole delocalization in the luminescent excited state of $CuInS_2$ NCs, estimated by Monte Carlo simulations to involve at most about four copper ions. These results provide unique insights into the luminescent excited states of these materials and they reinforce the description of $CuInS_2$ NCs as "heavily copper-doped NCs" in which photogenerated holes are rapidly localized in copper 3d-based orbitals.

KEYWORDS: *Copper indium sulfide, nanocrystal, photoluminescence, copper-doped, cation exchange, silver indium sulfide*

Ternary colloidal I−III−VI_2 nanocrystals (NCs) of copper and silver (e.g., $CuInS_2$, $AgInS_2$, etc.) have attracted broad attention as Cd/Pb-free nanophosphors and have stimulated interest in new applications enabled by their solution processability, high-photoluminescence quantum yields (PL QYs), and size-tunable band gap energies, such as full-spectrum lighting, luminescent solar concentration, and quantum dot (QD) photovoltaics.[1−10] Despite high interest, the complex defect chemistries and structural disorder of I−III−VI_2 NCs still present major challenges to understanding and controlling their physical properties. In particular, the microscopic PL mechanisms active in these ternary NCs are still debated. Here, we report combined synthetic, spectroscopic, and computational studies aimed at addressing the unique photophysical properties of luminescent I−III−VI_2 NCs, focusing particularly on identifying the contributions of copper to the luminescence of $Ag_{1-x}Cu_xInS_2$ NCs in the range $\sim 0 \leq x \leq \sim 1$.

An interesting development in recent years has been the recognition that $CuInS_2$ and copper-doped II−VI or III−V semiconductor NCs share nearly identical spectroscopic properties,[11,12] suggesting closely related PL mechanisms. For copper-doped semiconductor NCs, a great deal of evidence now points to a photophysical sequence in which NC photoexcitation leads to rapid hole capture by Cu^+, followed by slow radiative recombination of this deeply trapped hole with the delocalized conduction-band-like (CB-like) electron.[3] The electron in this scheme is subject to quantum confinement, affording tunability of this "free-to-bound" PL energy through NC size tuning or composition alloying. This mechanism in Cu^+-doped NCs has been demonstrated spectroscopically and by density functional theory (DFT),[12−15] and it also closely parallels the mechanism established in the classic G-Cu phosphor, Cu^+-doped ZnS (bulk).[3,16,17] Photogenerated holes also localize around the Ag^+ impurity ions of Ag^+-doped II−VI NCs, yielding many of the same spectroscopic characteristics found in analogous Cu^+-doped NCs, but the much larger second ionization energy of Ag^+ compared to Cu^+ results in inverted bonding and consequently hole wave functions that are dominated by silver-bound anion p orbitals rather than by the Ag(4d) orbitals themselves.[13]

For $CuInS_2$ and $AgInS_2$ NCs, the photoluminescence mechanisms are much less clear, and multiple plausible interpretations have been proposed.[1−3,9] Most descriptions of $CuInS_2$ NC PL invoke the well-known Donor−Acceptor Pair (DAP) recombination mechanism established for bulk $CuInS_2$. Various proposals describe carrier localization at lattice vacancies, antisite defects, or rare point defects.[2,9,11,18] Direct comparison[3] suggests that $CuInS_2$ NC PL actually has little in common with bulk $CuInS_2$ PL, however. Saturation of the band-edge TA bleach at relatively low excitation densities (only ~2 excitations/NC)[19,20] was interpreted as suggesting that at least one of the two charge carriers in the luminescent excited state occupies a delocalized quantized level, consistent

Received: December 7, 2018
Published: December 25, 2018

DOI: 10.1021/acs.nanolett.8b04905
Nano Lett. 2019, 19, 1318−1325

Scheme 1. Synthesis of $AgInS_2$ NCs and Their Conversion to $Ag_{1-x}Cu_xInS_2$ NCs ($\sim 0 \leq x \leq \sim 1$) by Partial Cation Exchange

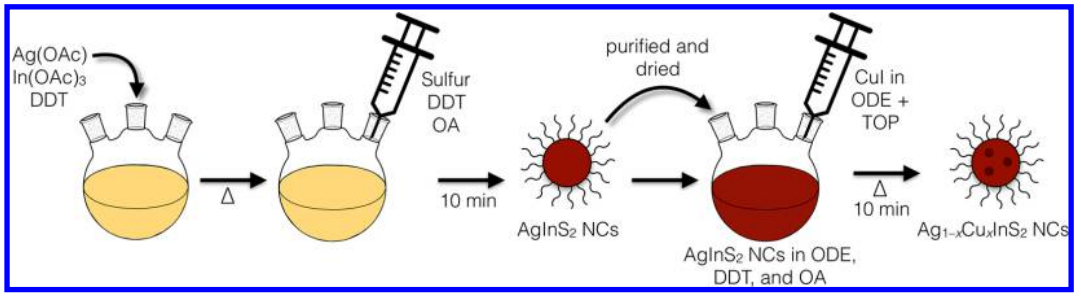

with the size dependence of the PL energy. The small degeneracy of this quantized level points to electron delocalization, and the large apparent Stokes shift then suggests deep hole trapping with various specific hole-trapping point defects considered as possibilities.[2,9,11] There is growing consensus that hole localization occurs at a Cu^+ ion,[3,12,21−26] often attributed to a rare lattice defect.

In one proposed mechanism, it has been suggested that holes rapidly localize at one or a few lattice Cu^+ ions in an exciton self-trapping process,[3,12] driven by localization forces including d-band potential fluctuations and a positive feedback between hole contraction and nuclear reorganization. In this mechanism, PL derived from radiative "free-to-bound" recombination of a self-trapped hole with a delocalized CB electron is characterized by a large Stokes shift and vibronically broadened band shape, directly analogous to the PL of Cu^+-doped semiconductor NCs[11,12] and bulk Cu^+-doped phosphors[3,16,17] as demonstrated experimentally. DFT studies of $CuInS_2$ and related NCs have described a strong propensity for hole localization even in the ordered chalcopyrite lattice structure, associated with the combination of poor d-band electronic coupling and electrostatic fluctuations.[25] By analogy to $CuInS_2$ NCs, the PL of $AgInS_2$ NCs is also frequently explained as DAP recombination[27−29] and has also been proposed[30] to involve exciton self-trapping.

We hypothesized that careful examination of a well-controlled series of $Ag_{1-x}Cu_xInS_2$ ($0 \leq x \leq 1$) NCs would offer a unique opportunity to isolate the impact of just the monovalent cation (Ag^+ or Cu^+), thereby clarifying the specific role that this cation plays in the PL of such NCs. Given the structural similarity of $CuInS_2$ and $AgInS_2$ NCs, it should be possible to prepare alloyed $Ag_{1-x}Cu_xInS_2$ NCs at any value of x between 0.00 and 1.00 by direct chemical means. Indeed, solid solutions of bulk $Ag_{1-x}Cu_xInSe_2$ show essentially no segregation effects.[31,32] Micro- and nanocrystalline $Ag_{1-x}Cu_xInS_2$ have already been examined for solar photocatalysis and photovoltaics, where alloying with $CuInS_2$ has proven useful for narrowing the $AgInS_2$ energy gap to access more solar photons,[33,34] and several studies have also described red-shifted PL upon incorporation of Cu^+ into $AgInS_2$ NCs.[35−37] Prior studies of $Ag_{1-x}Cu_xInS_2$ NCs have primarily explored the dilute Cu^+ regime ($x < \sim 0.25$), however, and their goals did not require controlling for NC size or shape variations that can also shift absorption and PL energies.

In the present study, partial Ag^+-to-Cu^+ cation exchange was used to prepare a homologous series of alloyed $Ag_{1-x}Cu_xInS_2$ NCs that spans from $x = 0$ to $x \sim 1$, all derived from the same parent $AgInS_2$ NCs (Scheme 1, see Methods for experimental details). A hallmark of NC cation-exchange chemistry is its preservation of the anion sublattice, such that the NCs retain their general size and shape during the transformation.[38−42] A collection of optical spectroscopic methods was then used to probe the evolution of NC electronic structure across this composition series. The experimental results are supplemented by DFT calculations that aid the data interpretation. Experimentally, the $Ag_{1-x}Cu_xInS_2$ NC PL energy is found to decrease rapidly upon addition of even small amounts of Cu^+ (small x), confirming direct participation of copper in the NC PL mechanism. DFT results show that dilute Cu^+ doping introduces discrete midgap Cu(3d) orbitals above the $AgInS_2$ NC valence band (VB) edge, similar to Cu^+-doped II−VI and III−V NCs, and consistent with hole trapping by copper in the luminescent excited states of these Cu^+-doped $AgInS_2$ NCs. Surprisingly, the $Ag_{1-x}Cu_xInS_2$ NC PL energy converges to the PL energy of $CuInS_2$ NCs at relatively small values of x (~ 0.20), remaining independent of x at larger values. This result is interpreted as reflecting detectable but very limited delocalization of photogenerated holes in the luminescent excited states of $Ag_{1-x}Cu_xInS_2$ NCs. Comparison of the data with Monte Carlo simulations suggests that photogenerated holes are trapped within small clusters of copper ions ($n \leq \sim 4$) in $Ag_{1-x}Cu_xInS_2$ NCs, even in the limit of $x = 1.00$ ($CuInS_2$). These results strongly support copper's role as the deep hole trap in both $Ag_{1-x}Cu_xInS_2$ and $CuInS_2$ NCs.

Figure 1A presents room-temperature absorption and continuous-wave (CW) PL spectra of representative $AgInS_2$ and $CuInS_2$ NCs with diameters of ~ 4 nm (synthesized independently, see Methods). Both NC samples show similar spectroscopic features: an absorption spectrum having a shoulder near its onset but lacking a clear maximum, and a broad, Stokes-shifted luminescence band. The absorption onset and PL maximum both occur at lower energies for the $CuInS_2$ NCs than for the $AgInS_2$ NCs. These results are consistent with analogous absorption and PL data reported previously for $CuInS_2$ and $AgInS_2$ NCs.[1−12,18−30,43,44]

Figure 1B summarizes absorption, PL, and transient-absorption (TA) spectroscopic results obtained for a series of $Ag_{1-x}Cu_xInS_2$ NCs with different x values ranging from 0.00 to 0.20, all prepared from the same starting $d = 3.9$ nm $AgInS_2$ NCs by partial cation exchange (Scheme 1). The PL quantum yields of these NCs are all similar, ranging from 32 to 44%. Like in Figure 1A ($AgInS_2$ and $CuInS_2$, or $x = 0$ and 1), increasing x decreases the absorption onset and PL energies. All three samples also show similar TA spectra featuring a broad bleach at the absorption edge and weak photoinduced absorption at lower energy within the gap. As described above, the bleach is attributable to the presence of delocalized CB electrons, and recent TA studies[26,45] of Cu^+:CdSe/CdS and $CuInS_2$ NCs have attributed a similar midgap photoinduced absorption signal to electronic transitions involving filling of copper-localized photogenerated holes, consistent with experimental photoinduced absorption measurements in bulk

DOI: 10.1021/acs.nanolett.8b04905
Nano Lett. 2019, 19, 1318−1325

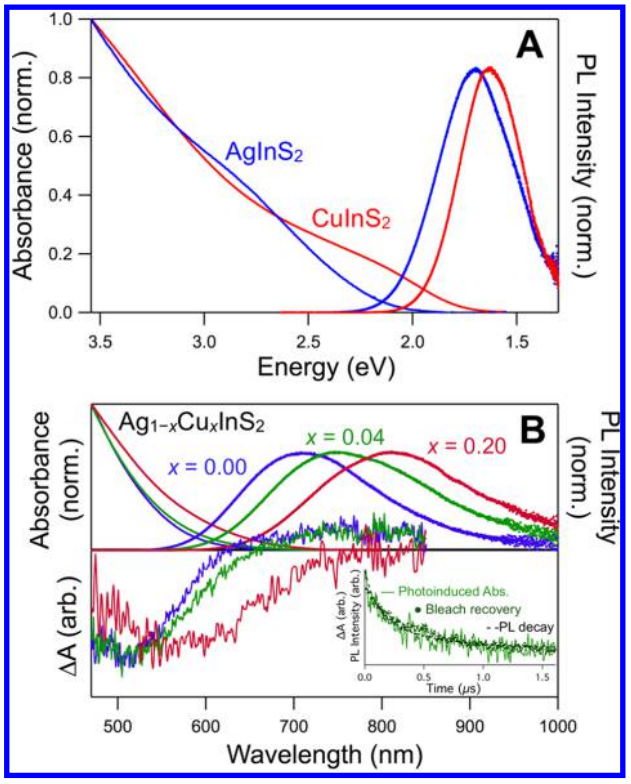

Figure 1. (A) Absorption and PL spectra of colloidal $AgInS_2$ NCs (blue) and $CuInS_2$ NCs (red) of similar sizes ($d \sim 4$ nm), suspended in toluene. (B) Absorption (top left), PL (top right), and TA (integrated between 0 and 300 ns, bottom) spectra of colloidal $Ag_{1-x}Cu_xInS_2$ NCs prepared by partial cation exchange from the same starting $d = 3.9$ nm $AgInS_2$ NCs. The blue traces show data for $x = 0.00$ (QY = 44%), the green traces show data for $x \sim 0.04$ (QY = 41%), and the red traces show data for $x \sim 0.20$ (QY = 32%). Inset: TA and PL decay dynamics associated with the $x \sim 0.04$ NCs shown in the main panel. The photoinduced absorption decay (green line, ~750 nm), the negative of the TA bleach recovery (dark green dots, ~500 nm), and the PL decay (dashed black line, 665–790 nm) all show similar dynamics with a time constant of ~400 ns, consistent with all three measurements probing decay of the same luminescent excited state. All measurements were performed on NCs in toluene at room temperature.

Cu^+:ZnS crystals[16] and theoretical predictions for absorption in Cu^{2+}:CdSe QDs.[14] The PL involves decay of both the electron and the hole. We note that similar TA data have also been interpreted to suggest that the luminescence of $CuInS_2$/ZnS NCs results from deep electron trapping rather than deep hole trapping, based in part on the observation that the photoinduced absorption dynamics are insensitive to a low-energy "dump" pulse.[18] In the present data, however, both the TA bleach and the photoinduced absorption show the same dynamics as the PL decay (inset, $\tau \sim 400$ ns), consistent with all three of these observables probing the same luminescent excited state.

Figure 2 plots absorption (normalized) and differential-absorption spectra collected for a much larger series of $Ag_{1-x}Cu_xInS_2$ NCs with different values of x, again all obtained from the same $d = 3.9 \pm 0.4$ nm $AgInS_2$ NCs by partial cation exchange with Cu^+. The average size and the size distribution remain essentially the same after copper incorporation (see Supporting Information (SI)). Figure 2A also presents normalized room-temperature PL spectra of these NCs. The

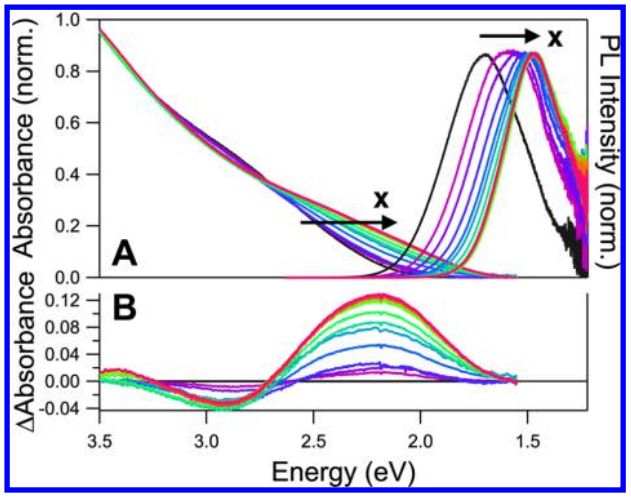

Figure 2. (A) Normalized absorption and PL spectra, and (B) differential absorption spectra of a series of $Ag_{1-x}Cu_xInS_2$ NCs with 0 (black) $\leq x \leq$ 0.9 (red). ΔAbsorbance was calculated as the absorption spectrum of each sample minus the starting absorption spectrum ($x = 0$). All data were collected at room temperature with the NCs in toluene. As x increases, new absorption grows in at ~2.2 eV, causing an apparent redshift of the absorption edge. The PL band maximum redshifts with increasing x. The absorption spectra are normalized at 3.54 eV.

arrows in Figure 2A indicate the trends with increasing x. As x increases, there is an apparent redshift of the absorption onset, but the differential absorption spectra in Figure 2B suggest that this change is better described as growth of distinct new absorption at a fixed energy (~2.2 eV) within the original $AgInS_2$ NC absorption gap. The amplitude of this new absorption grows with increasing x (see Supporting Information). Concomitantly, the PL band redshifts at small x but appears to become independent of x at larger values of x.

The changes in the absorption spectrum with increasing x are attributed to introduction of discrete new midgap states upon incorporation of Cu^+ into the $AgInS_2$ NC lattice. This interpretation is supported by DFT calculations on model $AgInS_2$ NCs. Figure 3 presents the near-gap molecular-orbital (MO) energies computed for several 34-cation $Ag_{1-x}Cu_xInS_2$ NCs having values of $x = 0.00$, 0.18, 0.47, and 1.00. The CB edge is set to 0 eV for all NCs to facilitate comparison. When $x = 0.00$ ($AgInS_2$), the VB edge is defined by a highest-occupied MO (HOMO) having ~66% S^{2-}(3p)-orbital character, with the remainder dominated by Ag^+(4d)-orbital character in an antibonding phase relationship with the S^{2-}(3p) orbitals. The corresponding bonding combination of Ag^+(4d) and S^{2-}(3p) orbitals occurs much deeper in energy. The CB edge is defined by a lowest-unoccupied MO (LUMO) that has ~50% In^{3+}(5s) character, with ~30% Ag^+(5s) character and ~15% S^{2-}(3p) character. These results agree well with those computed for bulk $AgInS_2$.[46−48]

Substituting a few Cu^+ ions into the $AgInS_2$ NC lattice introduces a discrete set of localized copper-centered orbitals just above the $AgInS_2$ VB edge. Increasing the copper content from $x = 0.18$ to 0.47 increases the number of these copper-based midgap orbitals but does not alter their energies substantially. As x is increased toward 1.00, these midgap orbitals evolve to become the VB edge of $CuInS_2$ NCs. For all copper-containing compositions, the HOMO has ~50–60% Cu^+(3d) character and substantial S^{2-}(3p) covalency. Across this series of $Ag_{1-x}Cu_xInS_2$ NCs, there is negligible change in

DOI: 10.1021/acs.nanolett.8b04905
Nano Lett. 2019, 19, 1318−1325

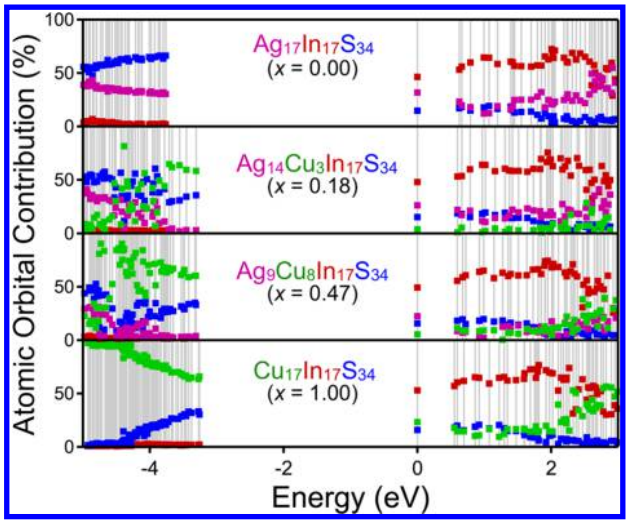

Figure 3. Molecular-orbital energies and atomic-orbital compositions of $Ag_{1-x}Cu_xInS_2$ NCs ($(Ag_{1-x}Cu_x)_{17}In_{17}S_{34}$, d ~1.6 nm, x = 0.00, 0.18, 0.47, 1.00) calculated by DFT. The specific clusters are indicated in each panel. Energies are referenced to the CB edge.

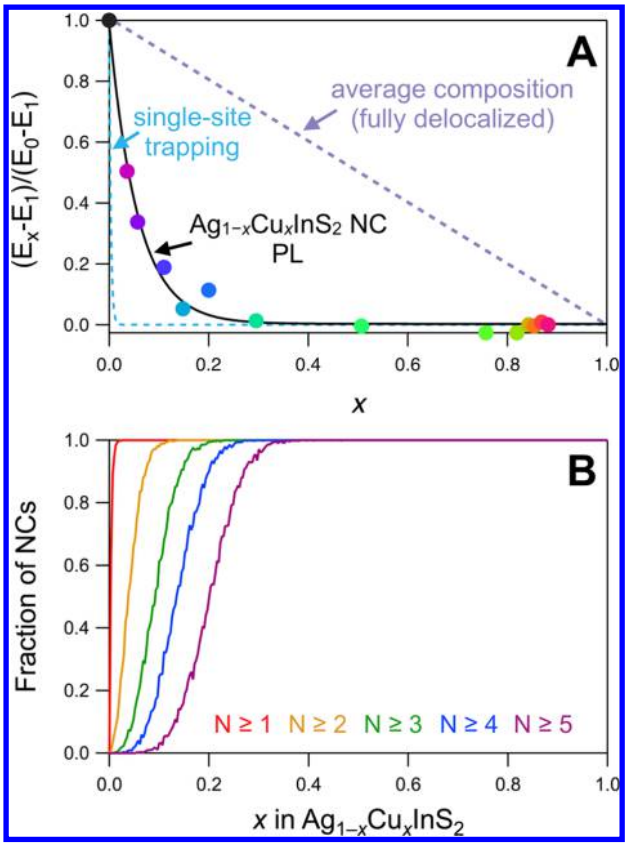

Figure 4. (A) Plot of PL energy shift (circles) versus x for the $Ag_{1-x}Cu_xInS_2$ NCs of Figure 2. The PL energy rapidly redshifts with small additions of copper until x ~ 0.20, beyond which it becomes independent of copper concentration. The black line is a guide to the eye. The blue dashed line shows the anticipated dependence of the PL energy on x for the scenario in which the hole in the luminescent excited state is completely localized on a single copper ion. The purple dashed line shows the anticipated dependence of the PL energy on x for the scenario in which the luminescent excited state is fully delocalized and experiences the average NC composition. (B) Statistics describing the probabilities of minimum Cu^+ cluster sizes in $Ag_{1-x}Cu_xInS_2$ NCs, computed by Monte Carlo methods for d = 4.05 nm NCs with ordered chalcopyrite lattice structures and plotted as a function of x. The curves illustrate the fraction of NCs possessing at least monomers ($N \geq 1$, red), nearest-neighbor dimers ($N \geq 2$, yellow), and clusters with 3 ($N \geq 3$, green), 4 ($N \geq 4$, blue), or 5 ($N \geq 5$, purple) of nearest-neighbor Cu^+ ions. At x = 0.2, nearly all NCs possess at least one cluster with N = 4 Cu^+ ions or larger.

the In^{3+} and S^{2-} contributions to the CB edge, and just the $Ag^+(5s)$ orbital contributions are replaced by $Cu^+(4s)$ contributions. Note that the midgap Cu^+ orbitals that appear in the dilute limit closely resemble the near-band-edge orbitals of the $CuInS_2$ NCs in both energy and composition, but simply occur with a much smaller density in the dilute-Cu^+ limit.

In the dilute-Cu^+ limit, the new $Cu^+(3d)$ orbitals above the $AgInS_2$ valence-band (VB) edge give rise to midgap electronic transitions involving promotion of a $Cu^+(3d)$ electron into the CB, i.e., a donor-type photoionization transition, also referred to as a metal-to-ligand (CB) charge-transfer ($ML_{CB}CT$) transition. The photogenerated hole in this $ML_{CB}CT$ excited state is localized at copper. Cu^+-doped $AgInS_2$ is thus directly analogous to other Cu^+-doped bulk and NC semiconductors, for which such midgap Cu^+ photoionization transitions are well characterized.[3,16,17] Increasing x in the $Ag_{1-x}Cu_xInS_2$ NC increases the $Cu^+(3d)$ density of states (Figure 3), consistent with the experimental observation (Figure 2B and SI) of growing midgap absorption with increasing x. As with the well-studied classic phosphor Cu^+:ZnS and various Cu^+-doped semiconductor NCs,[3,16,17] this $ML_{CB}CT$ excited state can return to the ground state via radiative free-to-bound recombination, generating broad midgap PL. Interestingly, the spectroscopically active orbitals at the absorption edge of $CuInS_2$ NCs (x = 1.0) are almost identical to those of Cu^+-doped $AgInS_2$ NCs in the dilute limit, consistent with the strong spectroscopic similarities between Cu^+-doped and $CuInS_2$ NCs noted previously.[3,11,12]

Although the experimental evolution of the absorption spectrum going from $AgInS_2$ to $CuInS_2$ NCs appears readily explained by these DFT results, the quantitative trend in the PL energies across the same series is more complex. Figure 4 summarizes the PL data from Figure 2 by plotting the PL energy shift versus x. This plot shows that the PL energy decreases with addition of Cu^+ until x ~ 0.20, but it then becomes independent of x between x = ~0.20 and 1.00. In other words, the PL spectra of homologous $Ag_{0.75}Cu_{0.25}InS_2$ and $CuInS_2$ NCs are indistinguishable even though their absorption spectra and VB-edge densities of states are very different. Increasing x beyond ~0.20 in $Ag_{1-x}Cu_xInS_2$ NCs thus does not simply shift the PL to lower energies in proportion to x, as observed for example in $Cd_{1-x}Zn_xSe$ alloy NCs (with minor bowing), where delocalized excitons experience the average crystal composition. The PL data also do not follow the trend expected in the scenario of hole localization at individual Cu^+ ions, however. In this scenario, only very small values of x (<~0.03) would be required to completely shift the PL to its new energy. Such a scenario is observed in Mn^{2+}-doped II–VI NCs, for example, where a single Mn^{2+} dopant is sufficient to completely shift the PL of a given NC to its new value, and increasing x has only a small additional effect. In contrast, the PL data in Figure 4A show that much larger values of x are required to reach the PL endpoint in the $Ag_{1-x}Cu_xInS_2$ NC series, despite the fact that the PL energy shifts rapidly even at very small x. At x = ~0.20, where the PL energy becomes independent of x, the average

DOI: 10.1021/acs.nanolett.8b04905
Nano Lett. 2019, 19, 1318–1325

NC possesses ~60 Cu^+ ions (see Supporting Information). We conclude that although the PL characteristics of $CuInS_2$ NCs are already fully evolved at Cu^+ levels far below x = 1.00, isolated Cu^+ impurity ions are not sufficient to make the PL of $Ag_{1-x}Cu_xInS_2$ NCs resemble that of $CuInS_2$ NCs.

It is conceivable that the results in Figure 4A could simply reflect the rare formation of some specific midgap trap state upon copper alloying, such as discussed in previous literature,[2,9,11] and that this trap is only present in every NC above $x \sim 0.20$. This interpretation is excluded by the observation that the PL spectra at intermediate compositions (~0.10) are not describable as linear combinations of the endpoint PL spectra (see Supporting Information). These data are thus inconsistent with the PL of $Ag_{1-x}Cu_xInS_2$ NCs coming from a specific rare defect.

We interpret the data in Figure 4A to suggest that holes localized at single copper dopants in the dilute Cu^+ limit ($x \sim 0$) can relax to lower energies by delocalizing over a larger number of copper impurity ions as x is increased, provided there exists sufficient intercopper electronic coupling. Such electronic coupling involves the copper 3d valence orbitals and is limited to nearest-neighbor interactions, i.e., hole delocalization requires the presence of nearest-neighbor copper ions. To analyze this scenario, the statistical spatial distributions of Cu^+ ions within the $Ag_{1-x}Cu_xInS_2$ NCs of Figures 2 and 4A were analyzed as a function of x using Monte Carlo methods. Figure 4B plots the fraction of NCs possessing at least Cu^+ monomers ($N \geq 1$), nearest-neighbor Cu^+ dimers ($N \geq 2$), trimers ($N \geq 3$), tetramers ($N \geq 4$), and larger clusters ($N \geq 5$) of nearest-neighbor Cu^+ ions as a function of x, computed for model d = 4.05 nm NCs with ordered chalcopyrite lattice structures. From these results, the fraction of NCs possessing at least one Cu^+ dopant increases very rapidly at small x such that no undoped NCs remain beyond $x \sim 0.03$. Likewise, the fraction of NCs possessing at least one Cu^+−Cu^+ nearest-neighbor interaction grows very rapidly with increasing x and reaches unity at $x \sim 0.12$. Both of these curves reach unity at values of x where the experimental PL energy still depends on x (Figure 4A), indicating that the PL energy is not determined by formation of either Cu^+ monomers or Cu^+−Cu^+ dimers within the NCs. Instead, the experimental NC PL energy only becomes independent of x at $x \geq$ ~0.20, where the majority of NCs possess clusters of at least three and possibly at least four nearest-neighbor Cu^+ ions. It is impossible to identify any specific cluster size or configuration that represents the limit of maximum hole delocalization, in part because multiple configurations exist for clusters of $N \geq 3$, but that complication does not preclude drawing the strong conclusion from this analysis that a small number of neighboring Cu^+ ions is necessary and sufficient to maximally stabilize the luminescent excited state in $Ag_{1-x}Cu_xInS_2$ NCs. Because the PL spectrum is the same at x = 1.00 ($CuInS_2$) as it is at x = ~0.25, the data presented here also provide compelling support for hole localization within small clusters of lattice Cu^+ ions in $CuInS_2$ NCs. Hole localization over small copper clusters within $CuInS_2$ NCs has also recently been predicted by DFT studies of the VB electronic structures of $Zn_{2(1-x)}(Cu,In)_xS_2$ NCs,[25] where the combination of weak copper d-band electronic coupling, electrostatic fluctuations, and electron−nuclear coupling was proposed to cause hole self-trapping even in point-defect-free ordered chalcopyrite NCs.

We note that the analysis of Figure 4B assumes random alloying of Cu^+ and Ag^+ in these $Ag_{1-x}Cu_xInS_2$ NCs. It is conceivable that thermodynamic forces could cause some degree of Cu^+ and Ag^+ segregation within the NCs; in such a scenario, copper clusters would form more rapidly with x than plotted in Figure 4B and slightly larger clusters would exist at any given x than predicted from the statistical analysis, but the same overall conclusion that holes delocalize over relatively small numbers of Cu^+ ions in $Ag_{1-x}Cu_xInS_2$ NCs would still be reached. Overall, these results and analysis reinforce the description of $CuInS_2$ NCs as "heavily copper-doped NCs," being more similar in electronic structure to sparsely Cu^+-doped NCs than to undoped II−VI or other semiconductor NCs that involve highly dispersive VBs.

Finally, we comment on relationships between the data and interpretations presented here and in related literature on $CuInS_2$ and copper-doped NCs. The description of the evolving electronic structure of $Ag_{1-x}Cu_xInS_2$ NCs with increasing x presented here is entirely consistent with the large body of literature on sparsely Cu^+-doped bulk and NC semiconductors,[3,16,17] which also show weak midgap $ML_{CB}CT$ absorption as well as broad, Stokes-shifted $ML_{CB}CT$ PL. For example, doping Cu^+ into CdSe NCs introduces new midgap $ML_{CB}CT$ absorption that scales with Cu^+ concentration, just like in Figure 2, as well as a similarly broad and Stokes-shifted PL spectrum.[49] In both $Ag_{1-x}Cu_xInS_2$ and Cu^+-doped CdSe NCs, the onset of the new $ML_{CB}CT$ absorption aligns with the PL origin, consistent with assignment of the PL as the corresponding $ML_{CB}CT$ free-to-bound recombination. $Ag_{1-x}Cu_xInS_2$ NCs with small x thus behave essentially the same as other sparsely Cu^+-doped NCs. Moreover, the growth of this midgap absorbance with increasing x in $Ag_{1-x}Cu_xInS_2$ NCs extends all the way to $CuInS_2$ NCs (x = 1.0), connecting the first absorption feature in $CuInS_2$ NCs with the $ML_{CB}CT$ absorption of sparsely Cu^+-doped semiconductor NCs.

The description of $Ag_{1-x}Cu_xInS_2$ NC PL presented here is also consistent with most interpretations of $CuInS_2$ NC PL,[3,12,21−26] which invoke hole trapping and radiative free-to-bound recombination. Like in Cu^+-doped NCs, the onset of absorption in $CuInS_2$ NCs overlaps the PL origin (Figure 1A), consistent with both measurements probing the same excited state, an interpretation bolstered by the observation that this lowest absorption band is bleached upon photoexcitation and recovers with the same dynamics as the PL decay (Figure 1B). These results appear inconsistent with "rare defect" interpretations of $CuInS_2$ NC PL, and instead suggest that this PL stems from localized $ML_{CB}CT$-type excited states involving lattice Cu^+ ions, as in self-trapped excitons. This conclusion is supported by the nearly indistinguishable magneto-optical and variable-temperature PL characteristics of Cu^+-doped and $CuInS_2$ NCs.[11,12]

Lastly, the conclusions presented here are not in conflict with effective-mass descriptions of $CuInS_2$ NC electronic structure,[50] which predict that the lowest-energy band-to-band excitation should be electric-dipole forbidden by parity selection rules. Two-photon absorption measurements[51] recently showed the existence of such a state but also showed that this state is too high in energy to explain the magnitude of the PL Stokes shifts observed in $CuInS_2$ NCs. The authors concluded that $CuInS_2$ NC PL must involve carrier trapping,[51] consistent with the interpretation presented here. We note that the multiband effective-mass model applied to describe the confined holes in $CuInS_2$ NCs assumed a spherical Hamiltonian and thus imposed a high-symmetry solution that cannot accommodate the symmetry breaking that

DOI: 10.1021/acs.nanolett.8b04905
Nano Lett. 2019, 19, 1318−1325

accompanies trapping. Atomistic DFT calculations on discrete $CuInS_2$ NCs have suggested that the VB edges of such NCs are very sensitive to symmetry-breaking electrostatic perturbations from defects or surfaces, making holes very susceptible to localization.[25] Our results and analysis are consistent with these atomistic DFT results.

In summary, the synthesis of a series of $Ag_{1-x}Cu_xInS_2$ NCs ($0 \leq x \leq 1$) by cation exchange starting from a single stock of $AgInS_2$ NCs has allowed the effects of copper on the absorption and PL spectroscopic properties of these NCs to be investigated systematically with minimal perturbation of other structural or compositional variables. These experiments reveal key aspects of the electronic structures of $Ag_{1-x}Cu_xInS_2$, including $CuInS_2$ NCs. Specifically, the results presented here demonstrate that addition of Cu^+ into $AgInS_2$ NCs introduces discrete, localized midgap Cu(3d) orbitals just above the $Ag_{1-x}Cu_xInS_2$ VB edge. These new orbitals in the dilute Cu^+ limit ($x \sim 0.00$) are very similar to the orbitals at the VB edge of $CuInS_2$ NCs ($x = 1.00$), as well as to the midgap orbitals of many other Cu^+-doped semiconductors. The NC PL energies show a striking trend of decreasing in energy with increasing x until ~0.20, beyond which they remain independent of x all the way up to $x = 1.00$. The absence of any x dependence of the PL energy between $x = \sim 0.20$ and 1.00 indicates limited hole delocalization in such NCs, including in $CuInS_2$ NCs ($x = 1.00$). This result in turn implies weak inter-Cu^+ electronic coupling relative to localization forces such as electron−nuclear coupling and electrostatic heterogeneity. Statistical modeling and analysis of the experimental data suggest that holes are delocalized over only around three or four copper ions in the luminescent excited state of $Ag_{1-x}Cu_xInS_2$ NCs with $x > \sim 0.20$, including $CuInS_2$ NCs, rather than being delocalized over the entire NC volume. These findings are consistent with exciton self-trapping in $CuInS_2$ NCs.[3,12,25] The results and analysis presented here advance our fundamental understanding of the electronic structures and excited-state properties of luminescent copper-doped and copper-based semiconductor NCs and help to inform the development of future photonic or energy-conversion technologies that employ such materials.

Methods. *Chemicals.* Sulfur powder (99.98%), indium(III) acetate (99.99%), 1-dodecaethiol (DDT; ≤98%), copper(I) iodide (CuI; 98%), oleic acid (OA; 90%), and 1-octadecene (ODE; 90%) were purchased from Aldrich. Silver acetate (99%) and trioctylphosphine (TOP; 97%) were purchased from STREM. All chemicals were used as received.

Nanocrystal Synthesis and Partial Cation Exchange. Silver indium sulfide NCs were synthesized according to the following procedure, which was adapted from a previous literature report.[27] To start, silver acetate (0.53 mmol), indium acetate (0.51 mmol), and DDT (83.3 mmol) were combined in a flask and stirred under nitrogen at 150 °C for 1 h. A separate, sulfur solution (sulfur (1.1 mmol), DDT (5.6 g), and OA (1.6 g)) was sonicated until all sulfur had dissolved (~30 min) and then purged with nitrogen for ~30 min. The sulfur precursor solution was then rapidly injected into the flask containing the silver, indium, and DDT precursors. The reaction was allowed to proceed for 10 min, at which point the flask was rapidly cooled. OA (~1 mL) was added to the flask at ~40 °C, after which point the flask continued to cool to room temperature. The NCs were washed twice with ethanol, methanol, and acetone, and then resuspended in hexanes and OA. The NCs were washed a third time with methanol and resuspended in toluene.

All $Ag_{1-x}Cu_xInS_2$ NCs were synthesized based on a procedure adapted from a previous synthetic method,[49] and the concentration of copper and TOP in the copper precursor solution was varied to obtain NCs with different values of x. A representative synthesis is as follows: briefly, preformed $AgInS_2$ NCs were dried and resuspended (with sonication) in 1.2 mL of DDT. Three milliliters of ODE and 0.1 mL of OA were added to the NC solution. The flask was heated to 60 °C, and three pump-purge cycles (20 min/cycle) were performed. A separate copper solution was also prepared for which 0.04 mmol CuI was dissolved in 12 mL of ODE, and the solution was purged for ~30 min, after which 0.02 mL of TOP (0.045 mmol) was added, and the solution was sonicated for ~60 min. The copper precursor solution (0.55 mL) was then swiftly injected into the flask containing the $AgInS_2$ NCs, and the reaction was allowed to proceed for 10 min. The flask was then quickly cooled to room temperature. The NCs were washed twice with ethanol and methanol, resuspending in toluene in between. The final product was resuspended in toluene. Concentrations of silver and copper in the NCs were determined by analysis of dried NCs digested in ultrapure nitric acid (EMD Chemicals) using inductively coupled plasma atomic emission spectrometry (ICP-AES; PerkinElmer).

Spectroscopic Measurements. Absorption spectra of the NCs were collected in toluene at room temperature using a Cary 5000 spectrophotometer (Varian). Continuous-wave (CW) photoluminescence (PL) spectra measurements were performed by exciting the colloidal NCs with a 405 nm laser diode and collecting the spectra using an OceanOptics 2000+ spectrometer. Transmission electron microscope (TEM) images were obtained using a FEI Tecnai G2 F20 operating at 200 kV, and size distribution analysis was performed on 115 individual NCs per sample. PL quantum yields were determined using an External Quantum Efficiency Measurement System with a Hamamatsu Integrating Sphere (C9920-12) and a Hamamatsu high-sensitivity photonic multichannel analyzer (C10027-01). Transient-absorption measurements were performed using an Ekspla Nd:YAG laser operating at a 25 Hz repetition rate. NCs were excited using the third harmonic of the 1064 nm fundamental with an excitation energy of ~100 μJ/pulse while stirring. A 150 W CW Xe lamp was used as the white-light probe source. The pump and probe beams intersected at a 90° angle. The dynamics and spectra were collected using a monochromator and streak camera with an instrument response of ~20 ps. All PL and TA dynamics are reported only on microsecond time scales, where any effects from Auger recombination are negligible. For this reason, the number of excitations per NC is ≤1 for all dynamics data presented here.

Density Functional Theory Calculations. DFT calculations were performed using Gaussian 09[52] with the PBE0 hybrid DFT functional[53,54] and the Los Alamos double-ζ pseudocore potential and corresponding basis set with explicit basis functions used to describe the S(3s, 3p), In(5s, 5p), Cu(3d, 4s, 4p), and Ag(4d, 5s, 5p) atomic orbitals.[55−57] This method has previously been applied to other doped NCs, including Cu^+:CdSe and Ag^+:CdSe NCs.[13,14,58] Small, roughly spherical NCs with 34 total cations (Cu^+, Ag^+, and In^{3+}) and 34 anions were constructed in the ordered chalcopyrite crystal structure; all NC geometries were optimized before other electronic-structure calculations were performed. Dangling bonds on

DOI: 10.1021/acs.nanolett.8b04905
Nano Lett. 2019, 19, 1318−1325

uncompensated surface ions were passivated by pseudohydrogen atoms with fractional charges (+1.25 for In^{3+}, +1.75 for Cu^{+} and Ag^{+}, and +0.5 for S^{2-}).[59,60]

Monte Carlo Calculations. A spherical $AgInS_2$ NC (d = 4.05 nm, 310 Ag^{+} cations) was constructed from the bulk $AgInS_2$ crystal structure. For each possible Cu^{+} dopant concentration with Cu^{+} substituting for Ag^{+} (x = 0/310, 1/310, 2/310...310/310), 1000 NCs were simulated. Because not all NCs in the experiment have identical numbers of dopants at a given ensemble dopant concentration, the actual number of dopants in each NC was selected from a Poissonian distribution around the average number of dopants at the given concentration. Dopants were randomly assigned to Ag^{+} cation sites, and the number and type of dopant clusters in each NC were determined. The data in Figure 4 represents the fraction of NCs (out of the 1000 simulated NCs) at each concentration that have at least one cluster of the specified size or larger.

■ ASSOCIATED CONTENT

Supporting Information

The Supporting Information is available free of charge on the ACS Publications website at DOI: 10.1021/acs.nanolett.8b04905.

Additional sample characterization (TEM, XRD), spectroscopic data (additional analysis of absorption spectra and PL decay times), and statistical calculations (PDF)

■ AUTHOR INFORMATION

Corresponding Author

*E-mail: gamelin@chem.washington.edu.

ORCID

Kira E. Hughes: 0000-0001-6454-8700

Sarah R. Ostheller: 0000-0001-8589-9227

Daniel R. Gamelin: 0000-0003-2888-9916

Notes

The authors declare no competing financial interest.

■ ACKNOWLEDGMENTS

This research was supported by the US National Science Foundation (NSF) through DMR-1807394 to D.R.G. The authors thank Dr. Sidney Creutz and Mr. Jose Araujo for collecting ICP and TEM data at the University of Washington's Molecular Analysis Facility, which is supported in part by funds from the UW Molecular Engineering and Sciences Institute, the UW Clean Energy Institute, the National Science Foundation, and the National Institutes of Health.

■ REFERENCES

(1) Aldakov, D.; Léfrançois, A.; Reiss, P. *J. Mater. Chem. C* **2013**, *1*, 3756−3776.

(2) Leach, A. D. P.; Macdonald, J. E. *J. Phys. Chem. Lett.* **2016**, *7*, 572−583.

(3) Knowles, K. E.; Hartstein, K. H.; Kilburn, T. B.; Marchioro, A.; Nelson, H. D.; Whitham, P. J.; Gamelin, D. R. *Chem. Rev.* **2016**, *116*, 10820−10851.

(4) Coughlan, C.; Ibáñez, M.; Dobrozhan, O.; Singh, A.; Cabot, A.; Ryan, K. M. *Chem. Rev.* **2017**, *117*, 5865−6109.

(5) Sandroni, M.; Wegner, K. D.; Aldakov, D.; Reiss, P. *ACS Energy Lett.* **2017**, *2*, 1076−1088.

(6) Li, L.; Daou, T. J.; Texier, I.; Chi, T. T. K.; Liem, N. Q.; Reiss, P. *Chem. Mater.* **2009**, *21*, 2422−2429.

(7) Knowles, K. E.; Kilburn, T. B.; Alzate, D.; McDowall, S.; Gamelin, D. R. *Chem. Commun.* **2015**, *51*, 9129−9132.

(8) Meinardi, F.; McDaniel, H.; Carulli, F.; Colombo, A.; Velizhanin, K. A.; Makarov, N. S.; Simonutti, R.; Klimov, V. I.; Brovelli, S. *Nat. Nanotechnol.* **2015**, *10*, 878−885.

(9) Leach, A. D. P.; Shen, X.; Faust, A.; Cleveland, M. C.; La Croix, A. D.; Banin, U.; Pantelides, S. T.; Macdonald, J. E. *J. Phys. Chem. C* **2016**, *120*, 5207−5212.

(10) Sumner, R.; Eiselt, S.; Kilburn, T. B.; Erickson, C.; Carlson, B.; Gamelin, D. R.; McDowall, S.; Patrick, D. L. *J. Phys. Chem. C* **2017**, *121*, 3252−3260.

(11) Rice, W. D.; McDaniel, H.; Klimov, V. I.; Crooker, S. A. *J. Phys. Chem. Lett.* **2014**, *5*, 4105−4109.

(12) Knowles, K. E.; Nelson, H. D.; Kilburn, T. B.; Gamelin, D. R. *J. Am. Chem. Soc.* **2015**, *137*, 13138−13147.

(13) Nelson, H. D.; Hinterding, S. O. M.; Fainblat, R.; Creutz, S. E.; Li, X.; Gamelin, D. R. *J. Am. Chem. Soc.* **2017**, *139*, 6411−6421.

(14) Nelson, H. D.; Li, X.; Gamelin, D. R. *J. Phys. Chem. C* **2016**, *120*, 5714−5723.

(15) Hassan, A.; Zhang, X.; Liu, X.; Rowland, C. E.; Jawaid, A. M.; Chattopadhyay, S.; Gulec, A.; Shamirian, A.; Zuo, X.; Klie, R. F.; Schaller, R. D.; Snee, P. T. *ACS Nano* **2017**, *11*, 10070−10076.

(16) Suzuki, A.; Shionoya, S. *J. Phys. Soc. Jpn.* **1971**, *31*, 1455−1461.

(17) *Phosphor Handbook*, second ed.; Yen, W. M., Shionoya, S., Yamamoto, H., Eds.; CRC Press: New York, 2007.

(18) Kraatz, I. T.; Booth, M.; Whitaker, B. J.; Nix, M. G. D.; Critchley, K. *J. Phys. Chem. C* **2014**, *118*, 24102−24109.

(19) Li, L.; Pandey, A.; Werder, D. J.; Khanal, B. P.; Pietryga, J. M.; Klimov, V. I. *J. Am. Chem. Soc.* **2011**, *133*, 1176−1179.

(20) Sun, J.; Zhu, D.; Zhao, J.; Ikezawa, M.; Wang, X.; Masumoto, Y. *Appl. Phys. Lett.* **2014**, *104*, No. 023118.

(21) Zang, H.; Li, H.; Makarov, N. S.; Velizhanin, K. A.; Wu, K.; Park, Y.-S.; Klimov, V. I. *Nano Lett.* **2017**, *17*, 1787−1795.

(22) van der Stam, W.; de Graaf, M.; Gudjonsdottir, S.; Geuchies, J. J.; Dijkema, J. J.; Kirkwood, N.; Evers, W. H.; Longo, A.; Houtepen, A. J. *ACS Nano* **2018**, *12*, 11244−11253.

(23) Fuhr, A. S.; Yun, H. J.; Makarov, N. S.; Li, H.; McDaniel, H.; Klimov, V. I. *ACS Photonics* **2017**, *4*, 2425−2435.

(24) Jara, D. H.; Stamplecoskie, K. G.; Kamat, P. V. *J. Phys. Chem. Lett.* **2016**, *7*, 1452−1459.

(25) Nelson, H. D.; Gamelin, D. R. *J. Phys. Chem. C* **2018**, *122*, 18124−18133.

(26) Berends, A. C.; Rabouw, F. T.; Spoor, F. C. M.; Bladt, E.; Grozema, F. C.; Houtepen, A. J.; Siebbeles, L. D. A.; de Mello Donegá, C. *J. Phys. Chem. Lett.* **2016**, *7*, 3503−3509.

(27) Hamanaka, Y.; Ogawa, T.; Tsuzuki, M.; Kuzuya, T. *J. Phys. Chem. C* **2011**, *115*, 1786−1792.

(28) Hamanaka, Y.; Ozawa, K.; Kuzuya, T. *J. Phys. Chem. C* **2014**, *118*, 14562−14568.

(29) Mao, B.; Chuang, C.-H.; Wang, J.; Burda, C. *J. Phys. Chem. C* **2011**, *115*, 8945−8954.

(30) Stroyuk, O.; Raevskaya, A.; Spranger, F.; Selyshchev, O.; Dzhagan, V.; Schulze, S.; Zahn, D. R. T.; Eychmüller, A. *J. Phys. Chem. C* **2018**, *122*, 13648−13658.

(31) Ciszek, T. F. *J. Cryst. Growth* **1986**, *79*, 689−694.

(32) Albornoz, J. G.; Serna, R.; León, M. *J. Appl. Phys.* **2005**, *97*, 103515.

(33) Tsuji, I.; Kato, H.; Kudo, A. *Chem. Mater.* **2006**, *18*, 1969−1975.

(34) Saha, S. K.; Guchhait, A.; Pal, A. J. *Phys. Chem. Chem. Phys.* **2014**, *16*, 4193−4201.

(35) Guchhait, A.; Pal, A. J. *ACS Appl. Mater. Interfaces* **2013**, *5*, 4181−4189.

(36) Chen, S.; Demillo, V.; Lu, M.; Zhu, X. *RSC Adv.* **2016**, *6*, 51161−51170.

DOI: 10.1021/acs.nanolett.8b04905
Nano Lett. 2019, 19, 1318−1325

(37) Raevskaya, A.; Rozovik, O.; Novikova, A.; Selyshchev, O.; Stroyuk, O.; Dzhagan, V.; Goryacheva, I.; Gaponik, N.; Zahn, D. R. T.; Eychmüller, A. *RSC Adv.* **2018**, *8*, 7550−7557.
(38) Son, D. H.; Hughes, S. M.; Yin, Y.; Alivisatos, A. P. *Science* **2004**, *306*, 1009−1012.
(39) Jain, P. K.; Amirav, L.; Aloni, S.; Alivisatos, A. P. *J. Am. Chem. Soc.* **2010**, *132*, 9997−9999.
(40) Groeneveld, E.; Witteman, L.; Lefferts, M.; Ke, X.; Bals, S.; Van Tendeloo, G.; de Mello Donega, C. *ACS Nano* **2013**, *7*, 7913−7930.
(41) Gupta, S.; Kershaw, S. V.; Rogach, A. L. *Adv. Mater.* **2013**, *25*, 6923−6944.
(42) De Trizio, L.; Manna, L. *Chem. Rev.* **2016**, *116*, 10852−10887.
(43) Cheng, K.-C.; Law, W.-C.; Yong, K.-T.; Nevins, J. S.; Watson, D. F.; Ho, H.-P.; Prasad, P. N. *Chem. Phys. Lett.* **2011**, *515*, 254−257.
(44) Knowles, K. E.; Kilburn, T. B.; Alzate, D. G.; McDowall, S.; Gamelin, D. R. *Chem. Commun.* **2015**, *51*, 9129−9132.
(45) Hughes, K. E.; Hartstein, K. H.; Gamelin, D. R. *ACS Nano* **2018**, *12*, 718−728.
(46) Liu, J.; Hua, E. *Mater. Sci. Semicond. Process.* **2015**, *40*, 446−452.
(47) Huang, D.; Persson, C. *Chem. Phys. Lett.* **2014**, *591*, 189−192.
(48) Sharma, S.; Verma, A. S.; Jindal, V. K. *Physica B* **2014**, *438*, 97−108.
(49) Yang, L.; Knowles, K. E.; Gopalan, A.; Hughes, K. E.; James, M. C.; Gamelin, D. R. *Chem. Mater.* **2016**, *28*, 7375−7384.
(50) Shabaev, A.; Mehl, M. J.; Efros, A. L. *Phys. Rev. B: Condens. Matter Mater. Phys.* **2015**, *92*, No. 035431.
(51) Nagamine, G.; Nunciaroni, H. B.; McDaniel, H.; Efros, A. L.; de Brito Cruz, C. H.; Padilha, L. A. *Nano Lett.* **2018**, *18*, 6353−6359.
(52) Frisch, M. J.; Trucks, G. W.; Schlegel, H. B.; Scuseria, G. E.; Robb, M. A.; Cheeseman, J. R.; Scalmani, G.; Barone, V.; Mennucci, B.; Petersson, G. A.; Nakatsuji, H.; Caricato, M.; Li, X.; Hratchian, H. P.; Izmaylov, A. F.; Bloino, J.; Zheng, G.; Sonnenberg, J. L.; Hada, M.; Ehara, M.; Toyota, K.; Fukuda, R.; Hasegawa, J.; Ishida, M.; Nakajima, T.; Honda, Y.; Kitao, O.; Nakai, H.; Vreven, T.; Montgomery, Jr., J. A.; Peralta, J. E.; Ogliaro, F.; Bearpark, M. J.; Heyd, J.; Brothers, E. N.; Kudin, K. N.; Staroverov, V. N.; Kobayashi, R.; Normand, J.; Raghavachari, K.; Rendell, A. P.; Burant, J. C.; Iyengar, S. S.; Tomasi, J.; Cossi, M.; Rega, N.; Millam, N. J.; Klene, M.; Knox, J. E.; Cross, J. B.; Bakken, V.; Adamo, C.; Jaramillo, J.; Gomperts, R.; Stratmann, R. E.; Yazyev, O.; Austin, A. J.; Cammi, R.; Pomelli, C.; Ochterski, J. W.; Martin, R. L.; Morokuma, K.; Zakrzewski, V. G.; Voth, G. A.; Salvador, P.; Dannenberg, J. J.; Dapprich, S.; Daniels, A. D.; Farkas, Ö.; Foresman, J. B.; Ortiz, J. V.; Cioslowski, J.; Fox, D. J. *Gaussian 09*; Gaussian, Inc.: Wallingford, CT, 2009.
(53) Perdew, J. P.; Burke, K.; Ernzerhof, M. *Phys. Rev. Lett.* **1996**, *77*, 3865−3868.
(54) Adamo, C.; Barone, V. *J. Chem. Phys.* **1999**, *110*, 6158−6170.
(55) Hay, P. J.; Wadt, W. R. *J. Chem. Phys.* **1985**, *82*, 299−310.
(56) Wadt, W. R.; Hay, P. J. *J. Chem. Phys.* **1985**, *82*, 284−298.
(57) Hay, P. J.; Wadt, W. R. *J. Chem. Phys.* **1985**, *82*, 270−283.
(58) Badaeva, E.; Feng, Y.; Gamelin, D. R.; Li, X. *New J. Phys.* **2008**, *10*, No. 055013.
(59) Huang, X.; Lindgren, E.; Chelikowsky, J. R. *Phys. Rev. B: Condens. Matter Mater. Phys.* **2005**, *71*, 165328.
(60) Wang, L.-W.; Li, J. *Phys. Rev. B: Condens. Matter Mater. Phys.* **2004**, *69*, 153302.

DOI: 10.1021/acs.nanolett.8b04905
Nano Lett. 2019, 19, 1318−1325